



HAL
open science

Spectral Analysis of the Martian Atmospheric Turbulence: InSight Observations

Orkun Temel, Cem Berk Senel, Aymeric Spiga, Naomi Murdoch, Don
Banfield, Ozgur Karatekin

► **To cite this version:**

Orkun Temel, Cem Berk Senel, Aymeric Spiga, Naomi Murdoch, Don Banfield, et al.. Spectral Analysis of the Martian Atmospheric Turbulence: InSight Observations. *Geophysical Research Letters*, 2022, 49, 10.1029/2022GL099388 . insu-03847106

HAL Id: insu-03847106

<https://insu.hal.science/insu-03847106>

Submitted on 10 Mar 2023

HAL is a multi-disciplinary open access archive for the deposit and dissemination of scientific research documents, whether they are published or not. The documents may come from teaching and research institutions in France or abroad, or from public or private research centers.

L'archive ouverte pluridisciplinaire **HAL**, est destinée au dépôt et à la diffusion de documents scientifiques de niveau recherche, publiés ou non, émanant des établissements d'enseignement et de recherche français ou étrangers, des laboratoires publics ou privés.

Geophysical Research Letters®

RESEARCH LETTER

10.1029/2022GL099388

Key Points:

- We make use of in-situ observations to investigate the Martian atmospheric turbulence
- We find distinct spectral behaviors of turbulence for daytime and nighttime conditions
- We report important effects of a regional dust storm and gravity wave activity on the turbulence energy cascade

Supporting Information:

Supporting Information may be found in the online version of this article.

Correspondence to:

O. Temel,
orkun.temel@oma.be

Citation:

Temel, O., Senel, C. B., Spiga, A., Murdoch, N., Banfield, D., & Karatekin, O. (2022). Spectral analysis of the Martian atmospheric turbulence: InSight observations. *Geophysical Research Letters*, 49, e2022GL099388. <https://doi.org/10.1029/2022GL099388>

Received 9 MAY 2022

Accepted 11 JUL 2022

Spectral Analysis of the Martian Atmospheric Turbulence: InSight Observations

Orkun Temel^{1,2} , Cem Berk Senel² , Aymeric Spiga^{3,4} , Naomi Murdoch⁵ , Don Banfield⁶, and Ozgur Karatekin²

¹KU Leuven, Institute of Astronomy, Leuven, Belgium, ²Royal Observatory of Belgium, Reference Systems and Planetology, Brussels, Belgium, ³Laboratoire de Météorologie Dynamique/Institut Pierre Simon Laplace (LMD/IPSL), Sorbonne Université, Centre National de la Recherche Scientifique (CNRS), École Polytechnique, Paris, France, ⁴Institut Universitaire de France, Paris, France, ⁵Institut Supérieur de l'Aéronautique et de l'Espace (ISAE-SUPAERO), Université de Toulouse, Toulouse, France, ⁶Cornell University, New York, NY, USA

Abstract In this study, we perform spectral analysis of Martian near-surface turbulence using the in-situ observations by NASA's InSight lander on Mars. A recent study on the daytime Martian boundary layer using the InSight observations showed that the conventional Kolmogorov energy cascade of inertial subrange fails to predict the spectral density of pressure (Banfield et al., 2020, <https://doi.org/10.1038/s41561-020-0544-y>). Here we extend this by investigating diurnal and seasonal variations in the spectral density of pressure, as the indicator of the Martian atmospheric turbulence. We show distinct spectral behaviors for the daytime and nighttime conditions. Moreover, we report the important effects of regional dust storms, gravity waves (GWs), bore, and solitary waves on the turbulent energy cascade. Our results show that the presence of a dust storm and GW activity can enhance the turbulence of the nighttime boundary layer of Mars despite the extreme stably stratified conditions compared to the terrestrial case.

Plain Language Summary Turbulent mixing in the first kilometers above the planetary surface, the atmospheric boundary layer, drives the transport of momentum, heat, and volatiles between a planet's surface and its atmosphere. Thus, it requires a detailed investigation by observations to be able to understand better the atmospheric dynamics, and most importantly, the processes controlling them. In this study, we make use of the InSight lander's pressure observations to understand how the Martian atmospheric turbulence differs over a daily cycle and in different seasons. Here we showed that the nocturnal near-surface environment of Mars can be more turbulent than thought before and it can have important implications for the Martian atmospheric seasonal cycles. We also find that the daytime and nocturnal turbulence exhibits different behaviors, which are affected by the presence of a regional dust storm and gravity wave activity.

1. Introduction

NASA's InSight (Interior exploration using Seismic Investigations, Geodesy and Heat Transport) mission landed in Elysium Planitia, a flat-smooth plain just north of the equator on Mars, on Mars year (MY) 34, after the Northern hemisphere Winter Solstice, $L_s = 295.5$ (November 26, 2018) (Banerdt et al., 2020). In addition to the interior structure, composition and thermal state of Mars, the InSight mission is devoted to a better understanding of near-surface atmospheric conditions (Banfield et al., 2020; Spiga et al., 2018, 2020), which are notably driven by the turbulent transport in the planetary boundary layer (PBL).

The Martian PBL is one important component of the Martian atmosphere, affecting the amount of dust lifted from its surface and altering the atmospheric dust cycle (Toigo et al., 2003), which leads to inter-annual and seasonal variations in the surface meteorological conditions (Montabone et al., 2015; Senel et al., 2021). Therefore, studying the Martian PBL is important to improve our understanding of the Martian climate. However, our current understanding of the Martian PBL mainly depends on the near-surface observations by previous landers (Hess et al., 1977; Martínez et al., 2009; Schofield et al., 1997; Taylor et al., 2008; Viúdez-Moreiras et al., 2019), which lacked either the accuracy, the continuity, or the high-frequency in-situ observations necessary to understand the turbulent energy cascade. Among the previous landers, only Viking (Chamberlain et al., 1976; Hess et al., 1977), Pathfinder (Schofield et al., 1997; Seiff et al., 1997), Phoenix (Holstein-Rathlou et al., 2010), and Mars Science Laboratory (MSL) (Gómez-Elvira et al., 2012; Viúdez-Moreiras et al., 2019) provided in-situ meteorological

data. However, their sampling frequency was limited up to 1, 0.25, 0.5, and 1 Hz, respectively. Unlike previous landers, the InSight lander can detect turbulent fluctuations continuously up to a pressure sampling frequency of 10 Hz (Banfield et al., 2019; Spiga et al., 2018). Moreover, the long temporal coverage of InSight allows us to investigate seasonal variations caused by the Martian dust cycle using a continuous high-resolution observational dataset. Here, we make use of high-frequency atmospheric pressure observations of InSight to analyze the slopes in the turbulent energy spectrum, and thus examine the deviations in the inertial exchange of energy between turbulence scales, falling through specific frequency ranges. Banfield et al. (2020) demonstrated that the slope in the energy spectrum of daytime pressure measured by InSight in the turbulent range is similar to Earth's and similarly at odds with theoretical expectations. This deserves further examination of the InSight data, including both nocturnal and daytime turbulence.

We focus on three main research questions: (a) How do the diurnal variations affect the turbulence energy spectrum on Mars? (b) What is the effect of atmospheric dust content? (c) Does gravity wave (GW) activity play an important role on the observed spectral slopes? We compute the turbulence spectrum for daytime and nocturnal (for two different local hour intervals, called as evening and nighttime) conditions. The turbulence spectrum shows the variation of the energy content for different frequency bands, which correspond to different turbulent length scales. For the spectral analysis of turbulence, Kolmogorov energy cascade is a widely-used, grounded theory that indicates a spectral slope of $-7/3$ for pressure fluctuations in the inertial subrange (Tsuji & Ishihara, 2003)—the range where the turbulence energy is conveyed from large to smaller eddies without dissipation. Despite the fact that the validity of Kolmogorov's energy cascade is also disputed for terrestrial boundary layers (Albertson et al., 1998), it is still used as a baseline for spectral analysis studies for turbulent boundary layers (Kunkel & Marusic, 2006; Tsuji et al., 2007).

It is worth noting that we define the inertial subrange as the spectral range, where the slope of the turbulence energy remains constant between the production and dissipation ranges. This definition, of course, is based on the equilibrium assumption that the net energy coming from large-scale eddies are in equilibrium with the energy transferred to small scale eddies. The constant slope falling to the frequency range between production-dissipation ranges may depart from Kolmogorov's theory, triggered by different atmospheric conditions in Mars case here or strong magneto-hydrodynamic turbulence in astrophysical or stellar flows (Beresnyak, 2014). However, those departures from theory may not violate the equilibrium assumption within the inertial subrange; therefore, the definition of inertial subrange would still be valid in those cases but showing different spectral slopes.

2. Data and Methodology

We make use of the data from InSight's pressure sensor, which performed observations up to a sampling frequency of 10 Hz after sol 168 and 2 Hz before sol 168, with noise levels of $10 \text{ mPa Hz}^{-0.5}$ and $50 \text{ mPa Hz}^{-0.5}$ between a range from 0.1 to 1 Hz, and at 0.01 Hz, respectively (Banfield et al., 2019). These sampling frequencies correspond to Nyquist frequencies ($f_{Nyq} = 0.5f_s$) of 5 and 1 Hz.

The sols on which we perform the spectral analysis are chosen based on the initial atmospheric results of the InSight lander (Banfield et al., 2020). First, we search for a sol without a regional dust storm and GW activity to be able to make distinction between the spectral behaviors of daytime and nighttime conditions, solely based on diurnal variations. Therefore, to investigate (a), we choose a sol without a regional dust storm (sol 18 after the landing). The difference in the spectral behavior of turbulence between daytime and nocturnal is related to the turbulent coherent structures. For (b), we focus on three sols before and during a regional dust storm (sols 18, 46, and 55). For (c), we investigate the sols with and without GW activity. For our observational analysis, we use a time window of 5 hr for daytime, evening, and nighttime conditions (corresponding to 11–16, 18–23, and 00–05 LMST).

We perform the spectral analysis using the Fourier transform from time to frequency domain. Suppose that a fluctuation series of pressure in the time domain is $p'(t)$. Then the series of turbulence fluctuations under consideration can be transformed from time, t , to frequency domain, ω , to possess the frequency distribution of turbulent energy content. Regarding this transform, the complex Fourier transform (also the fast Fourier transform – FFT algorithm) can be applied to $p'(t)$ to obtain $p'(\omega)$, then turbulence spectrum in the frequency domain, $E_{pp}(\omega) = p'(\omega)p'^*(\omega)$ in which the $p'^*(\omega)$ refers to the complex conjugate of $p'(\omega)$. By formulating the turbulence spectra as a function of frequency, large-scale eddies are represented in the lower frequency bands and the smaller eddies fall

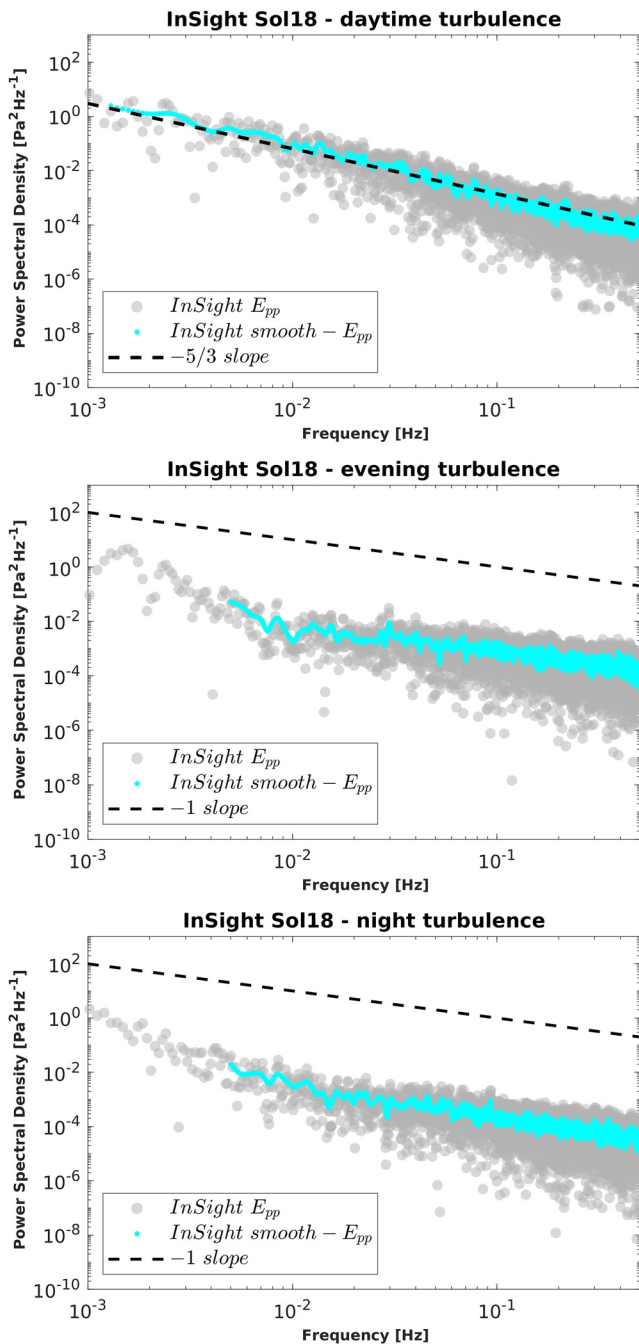


Figure 1. Turbulence spectra obtained by the InSight observations for different local times. The results are normalized with the maximum energy at the lowest frequency: (a) observations for daytime conditions, (b) observations for evening conditions, and (c) observations for nocturnal conditions.

are represented in the right side of the spectra within the inertial subrange. The higher the frequency, the higher is the effect of dissipation on the turbulence spectra. The inertial subrange refers to the range that the turbulence production conveys through the small and dissipative scales, in which the contribution of intermediate scales occurs. After the inertial range, the dissipative range lies. The typical time-scale for the dissipation range can be calculated as $(\nu/\epsilon)^{0.5}$, where ν is the kinematic viscosity and ϵ is the dissipation rate of turbulence kinetic energy. Using the published values of ϵ (Temel et al., 2021), this time scale is around 0.2 s. Therefore, the present

to the high frequency zone. Before using our spectral analysis methodology, we first perform a verification study by comparing our calculated spectral slope for daytime conditions with the one obtained by Banfield et al. (2020). As presented in Figure S1 in Supporting Information S1, we find a spectral slope of $-5/3 \approx -1.7$, consistent with the previously published result.

3. Diurnal Variations of Turbulence as Observed by the InSight Lander

First, we investigate how the turbulence energy spectrum varies during a sol, when neither a regional dust storm nor GW activity is present. Hence, we can interpret the differences we find in the observations solely as a result of diurnal variations in the radiative surface forcing. During the daytime conditions, the turbulent mixing in the boundary layer is enhanced as a result of surface heating, leading to strong vertical transport of momentum and heat, and forming larger convective structures (Kaimal et al., 1976; Schmidt & Schumann, 1989; Senel et al., 2019, 2020; Spiga et al., 2010, 2016; Temel et al., 2021). However, during the nocturnal conditions, convective turbulence is suppressed with the negative buoyancy flux, resulting from the surface cooling rate. Therefore, the scale of coherent structures in the stably stratified Martian PBL (hereafter SBL) is much smaller compared to the daytime PBL, similar to the terrestrial case (Mason & Derbyshire, 1990; Mayor, 2017).

As suggested by Banfield et al. (2020), the Martian SBL is exposed to intermittent turbulence, the irregular alteration of turbulence, similar to Earth's SBL. The difference between the terrestrial SBL and the Martian SBL is that the latter exhibits more intermittency due to its lower atmospheric density. Despite these similarities between the terrestrial and the Martian boundary layers, the Martian PBL can be regarded as an extreme state of the terrestrial boundary layer. This is a result of two main differences: (a) The lower atmospheric density yields higher variability in the turbulent winds to carry a similar heat flux, and thus leading to stronger pressure bursts as detected by the InSight lander (Banfield et al., 2020), which result in greater intermittency in the turbulence. (b) The Martian surface exhibits much stronger temperature swings compared to the surface of Earth as a result of lower thermal inertia. This leads to a higher level of turbulent mixing in the boundary layer during daytime conditions compared to Earth's PBL (Temel et al., 2021) and much stronger stable stratification during nighttime conditions (Petrosyan et al., 2011). Kolmogorov's theory of turbulence is proposed based on the assumption of isotropic turbulence, which falls from reality also for the case of Earth's PBL. The Martian PBL, being an extreme counterpart of the terrestrial PBL, is not likely to be explained by a theory grounded on isotropic turbulence.

In Figure 1, we investigate the pressure spectra for different local times, and the size of turbulent structures vary with diurnal radiative forcing. We formulated our spectral analysis based on frequency. Therefore, large-scale eddies, driven by the large-scale turbulent mixing in the PBL, fall to the lower frequency bands, through the production range, whereas the smaller eddies

spectral range (0.001 and 0.8 Hz) does not cover the dissipative range. Nevertheless, our resolution allows us to understand how the energy is transferred to the dissipative range by investigating the spectral slope within the inertial range.

We observe a shallower spectral slope for the daytime conditions, represented with a slope of $\eta = [-1.5, -1.7] \sim -5/3$, in comparison to the proposed slope of Kolmogorov's theory, $-7/3 = -2.33$. This disparity between the Kolmogorov's slope and the current observations shows that the intermediate scales act differently in the case of the Martian PBL, indicating lower energy content of turbulent fluctuations within the inertial subrange. This would imply attenuation of the energy transfer in the inertial subrange, from either large-to-small or small-to-large turbulence scales, subject to convective instabilities and strong wind gradients. Despite the smaller flow structures during the evening and nighttime conditions, the spectra exhibits substantially low energy content in comparison to daytime conditions. Such that the spectra has a slope of $\eta = -1$, following the dimensional analysis of Tchen (1954) on boundary-layer turbulence that gives -1 scaling in sheared flow. It is likely to be a result of intermittency. Due to intermittent turbulence, the nocturnal flow regime exhibits lower and sporadic turbulent mixing, thus weaker energy content, in which the transferred turbulent energy decays within the inertial subrange. Another possible underlying mechanisms can be linked to Kelvin Helmholtz instabilities (Iida & Nagano, 2007; Waite, 2011), which might also exist in planetary atmospheres (Johnson et al., 2014).

4. The Effect of a Regional Dust Storm

Figure 2 presents the time evolution of the turbulence energy cascade as observed by the InSight lander. In our spectral analysis, sol 18, 46, and 55 correspond to the observational time periods before, during its onset and the maxima of dust storm (see Figure 1c of Banfield et al. (2020)). For these sols, we used a sampling frequency of 2 Hz, which corresponds to the continuous frequency of the InSight pressure dataset before and after the dust storm season. However, as presented in Figure S2 in Supporting Information S1, a dataset with a higher sampling frequency, 10 Hz, provides consistent results with the ones obtained using a lower sampling frequency.

Before the dust storm, the inertial subrange exhibits the previously-illustrated slopes of $\eta = -5/3$ (daytime turbulence) and $\eta = -1$ (nocturnal turbulence). During the onset of the dust storm, despite the same behavior in the daytime energy spectra, evening spectra show an energy spike between the production and inertial ranges. Recent studies show that spatially-inhomogeneous distribution of dust can lead to higher levels of turbulence (Chatain et al., 2021; Wu et al., 2021), consistent with the present energy spike we observe during the onset of a dust storm. The observational studies using MSL/REMS data showed that during a regional dust storm, the vertical gradient of temperature decreases and leads to a weaker stability (Ordonez-Etxeberria et al., 2020). A recent study using the InSight lander's data show that this weaker stability, combining to low-level jets (LLJs) forming at night under dusty seasonal conditions, cause strong nighttime turbulence (Chatain et al., 2021). Therefore, another possible explanation of the energy spike found in the present paper might be the spectral trace of a LLJ, inducing energy production between the production and inertial ranges. Such an energy spike is not observed for the daytime conditions because the observed energy is much higher during the daytime so that such an additional input is negligible for daytime conditions. However, we find that this additional energy input is then rapidly dissipated in the evening spectra. Finally, we find that the additional energy injection is also present during the maxima of the dust storm for the daytime spectra. It causes an energy spike in the production range of spectrum, showing that dust-induced turbulent structures may act as the driving phenomena for the evening atmospheric surface layer.

5. The Effect of GW Activity

As shown in Figure 2 in the upper production range of evening and nighttime spectra, we observe a rapid decay of energy at lower frequencies below ~ 0.005 Hz. This spectral decay might be probing the existence of atmospheric GWs appearing through the evening and night at specific seasons at the InSight landing site, which were detected by making use of pressure and wind speed perturbations by impedance relation (see Methods-Gravity wave detection section in Banfield et al., 2020) occurring at the frequency range of several hundreds of seconds,

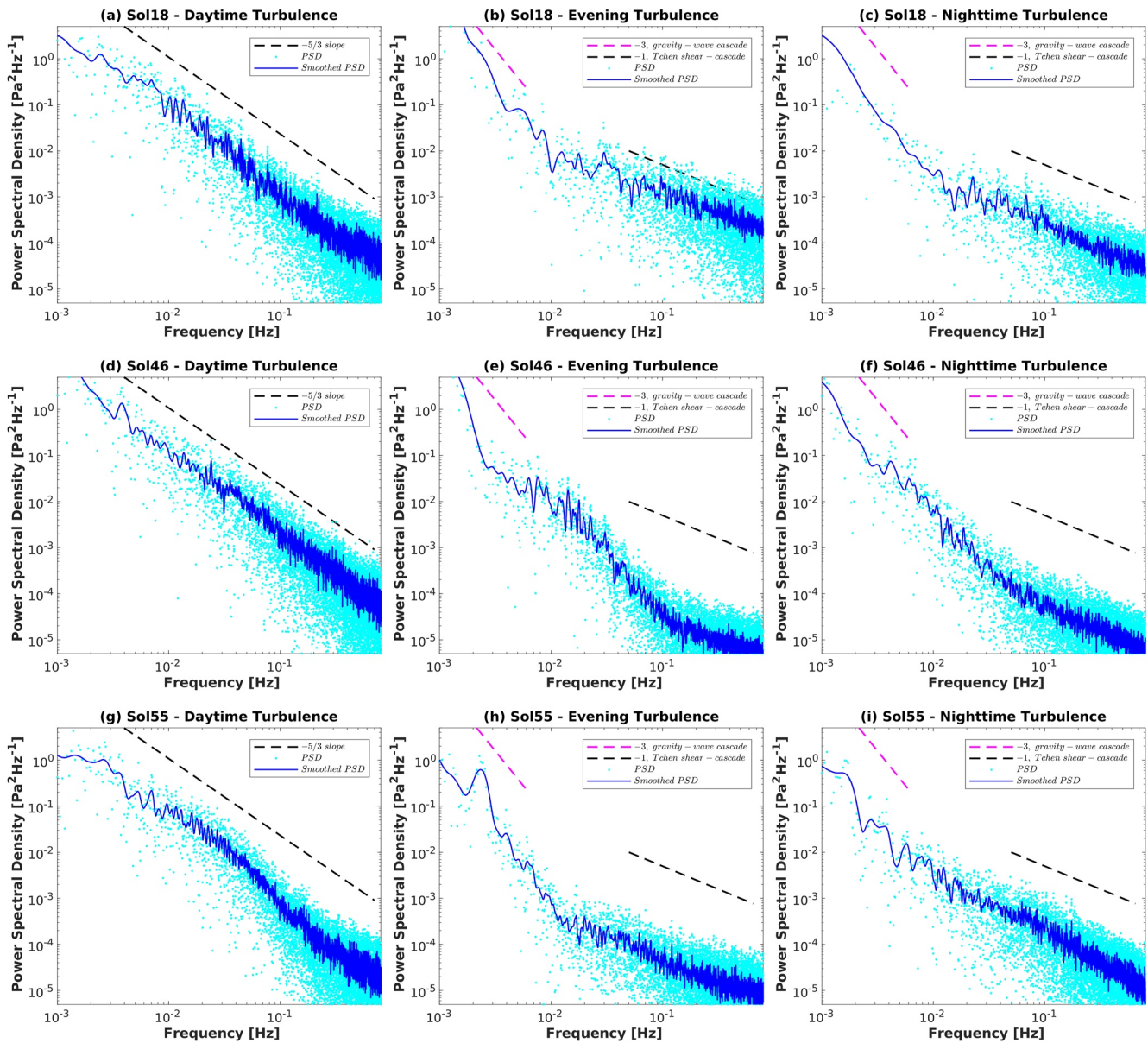


Figure 2. Turbulence spectra acquired by the InSight Observations before (sol 18, $L_s = 306^\circ$), during the onset (sol 46, $L_s = 323^\circ$), and at the climax of the dust storm (sol 55, $L_s = 328^\circ$). Sols are chosen based on the variation of dust opacity by the InSight lander (Banfield et al., 2020).

exhibiting the typical timescales of GWs (Fritts & Alexander, 2003; Gossard, 1962). The turbulent energy within the given frequency range decays rapidly with a spectral slope of $\eta \sim -3$, which agrees with the terrestrial GW cascade (Weinstock, 1978). However, a likely deviation from such a “near-universal” $\eta \sim -3$ spectra (Fritts, 1989; Fritts et al., 1988; Smith et al., 1987) may appear in certain conditions, especially due to the background winds for the atmosphere of Earth (Eckermann, 1995). Our results indicate that such departures from the “near-universal” $\eta \sim -3$ spectra could also be true for the Martian GWs. To illustrate, at the peak phase of the dust storm, that is, Sol46 (Figure 2e), the evening turbulence spectra shows even steeper slope than the $\eta \sim -3$ slope, cascading with the slope of $\eta \sim -4$. Such a tendency can be related to the strong background winds; thus intense shear instabilities, as a consequence of the peak dust storm activity at sol 46. However, this departure recovers back to $\eta \sim -3$ at sol 55 (during the local evening and night) when the dust storm terminates (Figures 2h and 2i). The gravity-wave signatures in our spectral-analysis are also consistent with the observations by Banfield et al. (2020), which reports that the first 150 sols after landing exhibit an intense gravity-wave activity covering the time period of

GW signatures probed here (i.e., sol 18, 46, and 55 in Figure 2). The other possible mechanism can be related to the difference between the energy content for daytime and nocturnal conditions. As presented in Figure 2, the upper production range contains a similar range of energy for daytime and nocturnal conditions but the nocturnal spectra reveals a much lower energy content within the inertial subrange consistent with the extreme diurnal atmospheric stability difference on Mars (Petrosyan et al., 2011).

In order to elaborate our analysis of the effect of GW activity and conclude whether this strong spectral slope of -3 is either a result of GW activity or a typical nocturnal turbulence signature for the Martian atmosphere, we investigate two types of GW activity types as classified by Banfield et al. (2020): (a) bores and solitary waves, where the pressure anomaly is denoted with a sudden strong peak in the variation of the evening pressure fluctuations and (b) regular GWs, where the amplitude of the pressure anomaly is weak but the fluctuations last for a much longer duration. By making use of the published catalog of atmospheric GWs as observed by the InSight lander (Banfield et al., 2020), we investigate the evening turbulence spectrum for six different sols and present in Figure 3 (left panel – bores and solitary waves, right panel – GWs). For the sols without any type of GW activity (sol 56, 82, and 152), we find that the upper production still contains the spectral slope of -3 , which leads to the conclusion that the rapid decay mechanism, denoted with a slope of -3 , is a result of the extreme daytime/nocturnal stability difference. However, we still observe important consequences of GW activity on the spectral dynamics of the Martian atmospheric turbulence. For the case of a strong GW activity, as in sol 124 and 135, the energy content in the upper-production range is amplified. Moreover, as in sol 65, this energy injection is even stronger for the case of solitary waves and bores, as a result of higher pressure fluctuations with respect to a regular GW so that the turbulence spectra shows even steeper spectral slope than -3 . This shows that the Martian nocturnal boundary layer may become more turbulent with the presence of a GW activity.

6. Conclusions and Possible Implications

Here, we present a spectral analysis of the in-situ observations of the InSight lander. In terms of the inertial subrange, we find that the daytime turbulence is governed with a slope of $-5/3$, and, the nocturnal turbulence consists of a slope of -1 , instead of $-7/3$ as suggested by Kolmogorov's energy cascade. The reported distinct behavior of daytime and nocturnal inertial subranges is due to the extreme stability difference in the Martian near-surface meteorological conditions. For daytime conditions, the deviation from Kolmogorov's theory is caused by the highly anisotropic nature of the Martian turbulence thanks to the high levels of turbulence kinetic energy. For the nocturnal conditions, it is linked to the intermittency and eddy bursts during night-time as shown in the present results. This implies that for future studies of the daytime Martian PBL, the contribution of large-scale eddies to turbulent transport, such as non-local transport (Ghannam et al., 2017), should be investigated. Moreover, the presence of intermittent eddy bursts can lead to sudden changes in the variation of the vertical wind, which can have important implications for nocturnal dust sedimentation. This also invokes a need for high temporal resolution observational studies of the variation of dust opacity on the Martian near-surface.

Based on our investigation of the effect of a regional dust storm on the energy cascade, we conclude that during the onset of a dust storm, additional energy is injected at the boundary between the production and inertial ranges. Moreover, we find that this injection can lead to sudden energy bursts in the energy spectra during the climax of the dust storm. This shows that, during dust storms, the nocturnal Martian PBL can be more turbulent despite the extreme stable stratification. During nocturnal conditions, increased nighttime turbulence is linked with higher shear production. For Earth's PBL, nocturnal BL with high shear production occurs with the formation of LLJs (Banta et al., 2002). LLJs are reinforced as a result of the dust cycle on Mars (Joshi et al., 1997). LLJs have important consequences for the transport of water on Earth (Higgins et al., 1997). Dust storm-induced LLJs on Mars can have important consequences for the transport of volatiles from the surface to the atmosphere. Similar to the effect of a regional dust storm, we find that GW activity leads to enhanced turbulence. This gravity-wave induced turbulence could affect the diurnal variation and the vertical transport of water, which drives the formation of boundary layer clouds on Mars (Daerden et al., 2010).

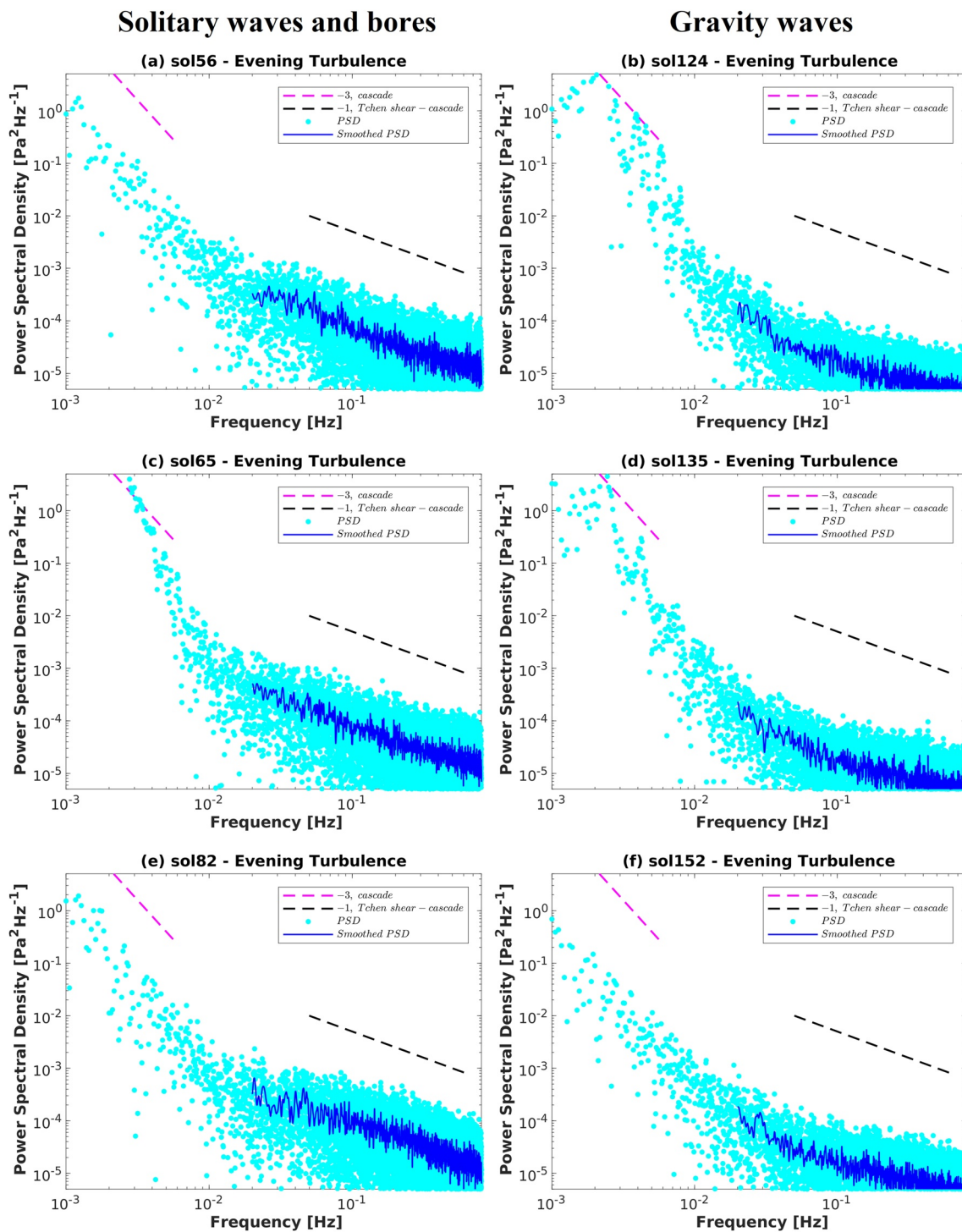


Figure 3. Turbulence spectra acquired for the days with and without solitary waves and bores (left panel, sol 65 with solitary wave and bores), and gravity waves (right panel, sol 124 and 135 with gravity waves). The sols are selected according to the gravity wave activity catalog acquired based on the InSight lander's pressure observations (Banfield et al., 2020).

Data Availability Statement

The InSight observations are available at https://atmos.nmsu.edu/data_and_services/atmospheres_data/INSIGHT/insight.html.

Acknowledgments

This work was financially supported by Grant 1ZZZL20N (to OT) of the Research Foundation Flanders. CBS was supported by the Belgian Science Policy Office (BELSPO) via Chicxulub BRAIN-be (Belgian Research Action through Interdisciplinary Networks) project. AS and NM thank CNES and ANR (ANR-19-CE31-0008-08) for their support. OK acknowledges the support of the BELSPO through the ESA/PRODEX Program. We acknowledge NASA, CNES, partner agencies and Institutions (UKSA, SSO, DLR, JPL, IPGP-CNRS, ETHZ, IC, MPS-MPG, ISAE), and the operators of JPL, SISMOC, MSDS, IRIS-DMC, and PDS for providing SEED data. This paper is InSight Contribution Number 225.

References

Albertson, J. D., Katul, G. G., Parlange, M. B., & Eichinger, W. E. (1998). Spectral scaling of static pressure fluctuations in the atmospheric surface layer: The interaction between large and small scales. *Physics of Fluids*, 10(7), 1725–1732. <https://doi.org/10.1063/1.869689>

Banerdt, W. B., Smrekar, S. E., Banfield, D., Giardini, D., Golombek, M., Johnson, C. L., et al. (2020). Initial results from the InSight mission on Mars. *Nature Geoscience*, 13, 183–189. <https://doi.org/10.1038/s41561-020-0544-y>

Banfield, D., Rodriguez-Manfredi, J., Russell, C., Rowe, K., Leneman, D., Lai, H., et al. (2019). InSight Auxiliary Payload Sensor Suite (APSS). *Space Science Reviews*, 215(1), 1–12. <https://doi.org/10.4324/9780429244575-1>

Banfield, D., Spiga, A., Newman, C., Forget, F., Lemmon, M., Lorenz, R., et al. (2020). The atmosphere of Mars as observed by InSight. *Nature Geoscience*, 13, 190–198. <https://doi.org/10.1038/s41561-020-0534-0>

Banta, R., Newsom, R., Lundquist, J., Pichugina, Y., Coulter, R., & Mahrt, L. (2002). Nocturnal low-level jet characteristics over Kansas during cases-99. *Boundary-Layer Meteorology*, 105(2), 221–252. <https://doi.org/10.1023/a:101992330866>

Beresnyak, A. (2014). Spectra of strong magnetohydrodynamic turbulence from high-resolution simulations. *The Astrophysical Journal Letters*, 784(2), L20. <https://doi.org/10.1088/2041-8205/784/2/L20>

Chamberlain, T., Cole, H., Dutton, R., Greene, G., & Tillman, J. (1976). Atmospheric measurements on Mars: The viking meteorology experiment. *Bulletin of the American Meteorological Society*, 57(9), 1094–1104. [https://doi.org/10.1175/1520-0477\(1976\)057<1094:amomtv>2.0.co;2](https://doi.org/10.1175/1520-0477(1976)057<1094:amomtv>2.0.co;2)

Chatain, A., Spiga, A., Banfield, D., Forget, F., & Murdoch, N. (2021). Seasonal variability of the daytime and nighttime atmospheric turbulence experienced by InSight on Mars. *Geophysical Research Letters*, 48(22), e2021GL095453. <https://doi.org/10.1029/2021gl095453>

Daerden, F., Whiteway, J., Davy, R., Verhoeven, C., Komguem, L., Dickinson, C., et al. (2010). Simulating observed boundary layer clouds on Mars. *Geophysical Research Letters*, 37(4). <https://doi.org/10.1029/2009gl014523>

Eckermann, S. D. (1995). Effect of background winds on vertical wavenumber spectra of atmospheric gravity waves. *Journal of Geophysical Research*, 100(D7), 14097–14112. <https://doi.org/10.1029/95jd00987>

Fritts, D. C. (1989). A review of gravity wave saturation processes, effects, and variability in the middle atmosphere. *Pure and Applied Geophysics*, 130(2), 343–371. https://doi.org/10.1007/978-3-0348-5825-0_14

Fritts, D. C., & Alexander, M. J. (2003). Gravity wave dynamics and effects in the middle atmosphere. *Reviews of Geophysics*, 41(1). <https://doi.org/10.1029/2001rg000106>

Fritts, D. C., Tsuda, T., Kato, S., Sato, T., & Fukao, S. (1988). Observational evidence of a saturated gravity wave spectrum in the troposphere and lower stratosphere. *Journal of the Atmospheric Sciences*, 45(12), 1741–1759. [https://doi.org/10.1175/1520-0469\(1988\)045<1741:oeoasg>2.0.co;2](https://doi.org/10.1175/1520-0469(1988)045<1741:oeoasg>2.0.co;2)

Ghannam, K., Duman, T., Salesky, S. T., Chamecki, M., & Katul, G. (2017). The non-local character of turbulence asymmetry in the convective atmospheric boundary layer. *Quarterly Journal of the Royal Meteorological Society*, 143(702), 494–507. <https://doi.org/10.1002/qj.2937>

Gómez-Elvira, J., Armiens, C., Castañer, L., Domínguez, M., Genzer, M., Gómez, F., et al. (2012). REMS: The environmental sensor suite for the Mars Science Laboratory Rover. *Space Science Reviews*, 170(1–4), 583–640. https://doi.org/10.1007/978-1-4614-6339-9_17

Gossard, E. E. (1962). Vertical flux of energy into the lower ionosphere from internal gravity waves generated in the troposphere. *Journal of Geophysical Research*, 67(2), 745–757. <https://doi.org/10.1029/jz067i02p00745>

Hess, S., Henry, R., Leovy, C. B., Ryan, J., & Tillman, J. E. (1977). Meteorological results from the surface of Mars: Viking 1 and 2. *Journal of Geophysical Research*, 82(28), 4559–4574. <https://doi.org/10.1029/jg082i28p04559>

Higgins, R., Yao, Y., Yarosh, E., Janowiak, J. E., & Mo, K. (1997). Influence of the Great Plains low-level jet on summertime precipitation and moisture transport over the central United States. *Journal of Climate*, 10(3), 481–507. [https://doi.org/10.1175/1520-0442\(1997\)010<0481:iotgpl>2.0.co;2](https://doi.org/10.1175/1520-0442(1997)010<0481:iotgpl>2.0.co;2)

Holstein-Rathlou, C., Gunnlaugsson, H., Merrison, J., Bean, K., Cantor, B., Davis, J., et al. (2010). Winds at the Phoenix landing site. *Journal of Geophysical Research*, 115(E5). <https://doi.org/10.1029/2009je003411>

Iida, O., & Nagano, Y. (2007). Effect of stable-density stratification on counter gradient flux of a homogeneous shear flow. *International Journal of Heat and Mass Transfer*, 50(1–2), 335–347. <https://doi.org/10.1016/j.ijheatmasstransfer.2006.06.022>

Johnson, J. R., Wing, S., & Delamere, P. A. (2014). Kelvin Helmholtz instability in planetary magnetospheres. *Space Science Reviews*, 184(1–4), 1–31. <https://doi.org/10.1007/s11214-014-0085-z>

Joshi, M. M., Haberle, R. M., Barnes, J. R., Murphy, J. R., & Schaeffer, J. (1997). Low-level jets in the NASA Ames Mars general circulation model. *Journal of Geophysical Research*, 102, 6511–6523. <https://doi.org/10.1029/96JE03765>

Kaimal, J., Wyngaard, J., Haugen, D., Coté, O., Izumi, Y., Caughey, S., & Readings, C. (1976). Turbulence structure in the convective boundary layer. *Journal of the Atmospheric Sciences*, 33(11), 2152–2169. [https://doi.org/10.1175/1520-0469\(1976\)033<2152:tsitcb>2.0.co;2](https://doi.org/10.1175/1520-0469(1976)033<2152:tsitcb>2.0.co;2)

Kunkel, G. J., & Marusic, I. (2006). Study of the near-wall-turbulent region of the high-Reynolds-number boundary layer using an atmospheric flow. *Journal of Fluid Mechanics*, 548, 375–402. <https://doi.org/10.1017/S0022112005007780>

Martínez, G., Valero, F., & Vázquez, L. (2009). Characterization of the Martian surface layer. *Journal of the Atmospheric Sciences*, 66(1), 187–198. <https://doi.org/10.1175/2008jas2765.1>

Mason, P., & Derbyshire, S. (1990). Large-eddy simulation of the stably-stratified atmospheric boundary layer. *Boundary-Layer Meteorology*, 53(1–2), 117–162. <https://doi.org/10.1007/bf00122467>

Mayor, S. D. (2017). Observations of microscale internal gravity waves in very stable atmospheric boundary layers over an orchard canopy. *Agricultural and Forest Meteorology*, 244, 136–150. <https://doi.org/10.1016/j.agrformet.2017.05.014>

Montabone, L., Forget, F., Millour, E., Wilson, R., Lewis, S., Cantor, B., et al. (2015). Eight-year climatology of dust optical depth on Mars. *Icarus*, 251, 65–95. <https://doi.org/10.1016/j.icarus.2014.12.034>

Ordonez-Etxeberria, I., Hueso, R., Sánchez-Lavega, A., & Vicente-Retortillo, Á. (2020). Characterization of a local dust storm on Mars with REMS/MSL measurements and MARCI/MRO images. *Icarus*, 338, 113521. <https://doi.org/10.1016/j.icarus.2019.113521>

Petrovsky, A., Galperin, B., Larsen, S. E., Lewis, S., Määttänen, A., Read, P., et al. (2011). The Martian atmospheric boundary layer. *Reviews of Geophysics*, 49(3). <https://doi.org/10.1029/2010rg000351>

Schmidt, H., & Schumann, U. (1989). Coherent structure of the convective boundary layer derived from large-eddy simulations. *Journal of Fluid Mechanics*, 200, 511–562. <https://doi.org/10.1017/s0022112089000753>

Schofield, J., Barnes, J. R., Crisp, D., Haberle, R. M., Larsen, S., Magalhaes, J., et al. (1997). The Mars Pathfinder atmospheric structure investigation/meteorology (ASI/MET) experiment. *Science*, 278(5344), 1752–1758. <https://doi.org/10.1126/science.278.5344.1752>

Seiff, A., Tillman, J. E., Murphy, J. R., Schofield, J. T., Crisp, D., Barnes, J. R., et al. (1997). The atmosphere structure and meteorology instrument on the Mars Pathfinder lander. *Journal of Geophysical Research*, 102(E2), 4045–4056. <https://doi.org/10.1029/96je03320>

Senel, C. B., Temel, O., Lee, C., Newman, C. E., Mischna, M. A., Muñoz-Esparza, D., et al. (2021). Interannual, seasonal and regional variations in the Martian convective boundary layer derived from GCM simulations with a semi-interactive dust transport model. *Journal of Geophysical Research: Planets*, 126(10), e2021JE006965. <https://doi.org/10.1029/2021je006965>

- Senel, C. B., Temel, O., Muñoz-Esparza, D., Parente, A., & van Beeck, J. (2020). Gray zone partitioning functions and parameterization of turbulence fluxes in the convective atmospheric boundary layer. *Journal of Geophysical Research: Atmospheres*, *125*(22), e2020JD033581. <https://doi.org/10.1029/2020jd033581>
- Senel, C. B., Temel, O., Porchetta, S., Muñoz-Esparza, D., & van Beeck, J. (2019). A new planetary boundary layer scheme based on LES: Application to the XPLA campaign. *Journal of Advances in Modeling Earth Systems*, *11*(8), 2655–2679. <https://doi.org/10.1029/2018ms001580>
- Smith, S. A., Fritts, D. C., & Vanzandt, T. E. (1987). Evidence for a saturated spectrum of atmospheric gravity waves. *Journal of the Atmospheric Sciences*, *44*(10), 1404–1410. [https://doi.org/10.1175/1520-0469\(1987\)044<1404:efasso>2.0.co;2](https://doi.org/10.1175/1520-0469(1987)044<1404:efasso>2.0.co;2)
- Spiga, A., Banfield, D., Teanby, N. A., Forget, F., Lucas, A., Kenda, B., et al. (2018). Atmospheric science with InSight. *Space Science Reviews*, *214*(7), 1–64. <https://doi.org/10.1007/s11214-018-0543-0>
- Spiga, A., Barth, E., Gu, Z., Hoffmann, F., Ito, J., Jemmett-Smith, B., et al. (2016). Large-eddy simulations of dust devils and convective vortices. *Space Science Reviews*, *203*(1–4), 245–275. <https://doi.org/10.1007/s11214-016-0284-x>
- Spiga, A., Forget, F., Lewis, S., & Hinson, D. (2010). Structure and dynamics of the convective boundary layer on Mars as inferred from large-eddy simulations and remote-sensing measurements. *Quarterly Journal of the Royal Meteorological Society*, *136*(647), 414–428. <https://doi.org/10.1002/qj.563>
- Spiga, A., Murdoch, N., Lorenz, R., Forget, F., Newman, C., Rodriguez, S., et al. (2020). A study of daytime convective vortices and turbulence in the Martian planetary boundary layer based on half-a-year of insight atmospheric measurements and large-eddy simulations. *Journal of Geophysical Research: Planets*, *126*(1), e2020JE006511. <https://doi.org/10.1029/2020JE006511>
- Taylor, P. A., Catling, D. C., Daly, M., Dickinson, C. S., Gunnlaugsson, H. P., Harri, A.-M., & Lange, C. F. (2008). Temperature, pressure, and wind instrumentation in the phoenix meteorological package. *Journal of Geophysical Research*, *113*(E3). <https://doi.org/10.1029/2007je003015>
- Tchen, C.-M. (1954). Transport processes as foundations of the Heisenberg and Obukhoff theories of turbulence. *Physical Review*, *93*(1), 4. <https://doi.org/10.1103/physrev.93.4>
- Temel, O., Senel, C. B., Porchetta, S., Muñoz-Esparza, D., Mischna, M. A., Van Hoolst, T., et al. (2021). Large eddy simulations of the Martian convective boundary layer: Towards developing a new planetary boundary layer scheme. *Atmospheric Research*, *250*, 105381. <https://doi.org/10.1016/j.atmosres.2020.105381>
- Toigo, A. D., Richardson, M. I., Ewald, S. P., & Gierasch, P. J. (2003). Numerical simulation of Martian dust devils. *Journal of Geophysical Research*, *108*(E6), 5047. <https://doi.org/10.1029/2002je002002>
- Tsuji, Y., Fransson, J. H., Alfredsson, P. H., & Johansson, A. V. (2007). Pressure statistics and their scaling in high-Reynolds-number turbulent boundary layers. *Journal of Fluid Mechanics*, *585*, 1. <https://doi.org/10.1017/s0022112007006076>
- Tsuji, Y., & Ishihara, T. (2003). Similarity scaling of pressure fluctuation in turbulence. *Physical Review E*, *68*(2), 026309. <https://doi.org/10.1103/physreve.68.026309>
- Viúdez-Moreiras, D., Gómez-Elvira, J., Newman, C., Navarro, S., Marin, M., Torres, J., et al. (2019). Gale surface wind characterization based on the Mars Science Laboratory REMS dataset. Part I: Wind retrieval and Gale's wind speeds and directions. *Icarus*, *319*, 909–925. <https://doi.org/10.1016/j.icarus.2018.10.011>
- Waite, M. L. (2011). Stratified turbulence at the buoyancy scale. *Physics of Fluids*, *23*(6), 066602. <https://doi.org/10.1063/1.3599699>
- Weinstock, J. (1978). On the theory of turbulence in the buoyancy subrange of stably stratified flows. *Journal of the Atmospheric Sciences*, *35*(4), 634–649. [https://doi.org/10.1175/1520-0469\(1978\)035<0634:ottoti>2.0.co;2](https://doi.org/10.1175/1520-0469(1978)035<0634:ottoti>2.0.co;2)
- Wu, Z., Richardson, M. I., Zhang, X., Cui, J., Heavens, N. G., Lee, C., et al. (2021). Large eddy simulations of the Dusty Martian convective boundary layer with MarsWRF. *Journal of Geophysical Research: Planets*, *126*(9), e2020JE006752. <https://doi.org/10.1029/2020je006752>